Follicular dendritic cells control engulfment of apoptotic bodies by secreting Mfge8

Jan Kranich,[1] Nike Julia Krautler,[1] Ernst Heinen,[3]
Magdalini Polymenidou,[1] Claire Bridel,[1] Anita Schildknecht,[2]
Christoph Huber,[4] Marie H. Kosco-Vilbois,[5] Rolf Zinkernagel,[2]
Gino Miele,[6] and Adriano Aguzzi[1]

[1]Institute of Neuropathology and [2]Institute of Experimental Immunology, University Hospital of Zurich,
 8091 Zurich, Switzerland
[3]Institute of Human Histology, University of Liège, 4000 Liège, Belgium
[4]Department of Immunology, The Scripps Research Institute, La Jolla, CA 92037
[5]NovImmune SA, 1211 Geneva, Switzerland
[6]Translational Medicine Research Collaboration, Sir James Black Centre, University of Dundee, Dundee DD1 5EH, Scotland, UK

The secreted phosphatidylserine–binding protein milk fat globule epidermal growth factor 8 (Mfge8) mediates engulfment of apoptotic germinal center B cells by tingible-body macrophages (TBMϕs). Impairment of this process can contribute to autoimmunity. We show that Mfge8 is identical to the mouse follicular dendritic cell (FDC) marker FDC-M1. In bone-marrow chimeras between wild-type and $Mfge8^{-/-}$ mice, all splenic Mfge8 was derived from FDCs rather than TBMϕs. However, $Mfge8^{-/-}$ TBMϕs acquired and displayed Mfge8 only when embedded in $Mfge8^{+/+}$ stroma, or when situated in lymph nodes draining exogenous recombinant Mfge8. These findings indicate a licensing role for FDCs in TBMϕ-mediated removal of excess B cells. Lymphotoxin-deficient mice lacked FDCs and splenic Mfge8, and suffer from autoimmunity similar to $Mfge8^{-/-}$ mice. Hence, FDCs facilitate TBMϕ-mediated corpse removal, and their malfunction may be involved in autoimmunity.

CORRESPONDENCE
Adriano Aguzzi:
Adriano.Aguzzi@usz.ch

Follicular DCs (FDCs) reside in primary B cell follicles and germinal centers (GCs) (1). FDCs retain native immune complexes with complement and Fcγ receptors (2), and display them to B cells, which they embrace with intricate dendritic networks. This is thought to facilitate the GC reactions, and the selection of B cells that gives rise to high-affinity antibodies (3) and long-term memory B cells (4). But others (5) have questioned the importance of FDCs because primary immune responses, affinity maturation, and memory B cells arise in mice engineered to lack the retention of immune complexes by FDCs (6), and even in $Lta^{-/-}$ mice that are deficient in lymphotoxin (LT) signaling and lack FDCs completely (7). Hence, the functional contribution of FDCs to affinity maturation remains unclear.

Some biomarkers, including the complement receptors CD21/35 and the complement factor C4 (8), allow for FDC immunodetection in vivo, yet none of them are exclusively restricted to FDCs. A more specific marker is hybridoma clone 4C11, whose reactivity is confined to FDCs and tingible-body macrophages (TBMϕs) (9). The antigen recognized by 4C11 was provisionally termed FDC-M1, but its identity has remained unknown.

Phagocytosis of apoptotic GC B cells, the remnants of which are recognizable as tingible bodies inside TBMϕs, is thought to be a crucial function of TBMϕs. Apoptotic cells are engulfed upon opsonization by milk fat globule epidermal growth factor (EGF) 8 (Mfge8) (10), which binds bifunctionally to phosphatidylserine on apoptotic cells and to integrins expressed by phagocytes (11). Originally identified as a membrane component of milk-fat globules (12), $Mfge8$ was reported to be expressed by various phagocytes, including TBMϕs, activated peritoneal macrophages (PMϕs), and immature DCs (10, 11).

$Mfge8^{-/-}$ mice suffer from impaired engulfment of GC B cell corpses by TBMϕs. Consequently, their TBMϕs carry supernumerary nonengulfed apoptotic B cells, which cause

The online version of this article contains supplemental material.

them to appear enlarged. This defect is associated with systemic lupus erythematosus (SLE) and autoimmune glomerulonephritis (10). In this report, we provide conclusive evidence that the FDC-M1 antigen identified by clone 4C11 is identical to Mfge8, that FDCs are the only source of splenic Mfge8, and that TBMφs only acquire surface Mfge8 if situated in the proximity of *Mfge8*-expressing FDCs or in lymph nodes that drain exogenous Mfge8. The absence of FDCs in mice lacking LTs or their receptors correlated with the profound depletion of splenic Mfge8 in LT-deficient mice, suggesting that impairment of FDC homeostasis contributes to their autoimmune pathologies.

RESULTS AND DISCUSSION
FDC–M1 and Mfge8 are identical
The present report originated from our serendipitous observation that FDC-M1$^+$ networks were completely absent from splenic cryosections of *Mfge8*$^{-/-}$ mice stained with anti–FDC-M1 antibody 4C11 (Fig. S1, available at http://www.jem.org/cgi/content/full/jem.20071019/DC1). This was unexpected, because no FDC abnormalities had been reported in *Mfge8*$^{-/-}$ mice despite progressive splenomegaly, enlarged splenic TBMφs, and hyperplastic follicles with increased numbers of peanut agglutinin–positive (PNA$^+$) GCs (10). The absence of 4C11 immunoreactivity in *Mfge8*$^{-/-}$ spleens did not result from an absence of mature FDCs, because FDC networks were easily identifiable by CD21/35 immunostains (Fig. S1).

The anti-Mfge8 antibodies 18A2-G10 and 2422 (11) identified FDC networks and colocalized with 4C11 immunostains (Fig. 1 A). We therefore considered the possibility that FDC-M1 and Mfge8 are the same antigen. Indeed, preincubation with excess rMfge8, but not with rEGF or recombinant prion protein (rPrP), inhibited the binding of both 18A2-G10 and 4C11 to FDC networks. The presence of FDCs in these sections was independently confirmed by PrP^C-specific immunolabeling, which is abundantly expressed by FDCs (13) (Fig. 1 B).

We then assessed whether anti–FDC-M1 antibody 4C11 immunoprecipitates Mfge8. Paramagnetic beads were conjugated to immunoaffinity-purified antibodies 4C11, anti-Mfge8 antibody 2422, or rat IgG2c isotype control antibody. Beads were incubated with protein extracts from WT or *Mfge8*$^{-/-}$ spleens, and precipitated proteins were analyzed by Western blotting with anti-Mfge8 antibody 18A2-G10. After immunoprecipitation with anti-Mfge8 antibodies, two bands with molecular masses of ∼45 and 55 kD were detected (Fig. 1 C). After immunoprecipitation with anti–FDC-M1 beads, two signals were obtained with molecular masses matching those of the 2422 immunoprecipitation (Fig. 1 C). Both signals were absent in spleens from *Mfge8*$^{-/-}$ mice, confirming their identity as genuine Mfge8.

We next verified the interaction of rMfge8 with anti–FDC-M1 antibody 4C11 by surface plasmon resonance (SPR). 4C11 was injected onto Biacore sensor chip surfaces covalently coated with rMfge8 or, for control, rPrP. Inter-

action of 4C11 with immobilized rMfge8 was observed over several serial injections until binding had reached saturation (Fig. 1 D, I). When anti-Mfge8 antibody 2422 was subsequently injected, its binding was minimal (Fig. 1 D, I, arrow, 2422), suggesting that 4C11 interfered with the binding of 2422 to rMfge8. Binding of anti-Mfge8 antibody 18A2-G10, in contrast, was not affected (Fig. 1 D, I, arrow, 18A2-G10). Rat IgG2c did not interact with immobilized rMfge8 (not depicted).

Antibodies were then reinjected in a different order. First, 2422 was added until saturation was reached (Fig. 1 D, II). 4C11 was injected, yet it did not bind to rMfge8 (Fig. 1 D, II, arrow, 4C11). In contrast, 18A2-G10 always bound to rMfge8, even in the presence of previously bound 2422 or 4C11 (Fig. 1 D, I and II). Hence, the 18A2-G10 epitope is distinct from those of the other two antibodies. These results indicate that 4C11 and 2422 abrogate each other's binding to Mfge8, either because they share a common or overlapping epitope, or because they sterically hinder each other. This was confirmed by the next experiment: immobilized 18A2-G10 was used to capture rMfge8. Then, the antibodies 18A2-G10, 2422, and 4C11 were added in a sandwich design. Under these conditions, injected 18A2-G10 did not bind to surfaces decorated with 18A2-G10–captured rMfge8, confirming that 18A2-G10 binds to a single epitope on Mfge8 (Fig. 1 D, III). Subsequent injection of 4C11 resulted in a strong interaction with captured rMfge8. When 2422 was applied, no binding occurred. We then reversed the order of injections: 2422 was added before 4C11. In this case, the first antibody, 2422, interacted with 18A2-G10–captured rMfge8, whereas 4C11 did not (Fig. 1 D, IV).

These data show that the FDC-M1 antigen identified by antibody 4C11 is Mfge8. The molecular identification of FDC-M1 expands the arsenal of tools for functional and morphological studies of FDCs in many ways. Because Mfge8 is secreted, its histological assignment by RNA in situ hybridization (ISH) is more informative of its cellular origin than immunohistology and will help define the precise histogenesis of FDCs. Also, we found that anti-Mfge8 antibody 18A2-G10 labels FDCs on formalin-fixed, paraffin-embedded tissue (unpublished data), thereby enabling the recognition of FDCs in archived tissue.

FDCs are the major source of Mfge8 in the spleen
The finding that Mfge8 is detected in TBMφs within splenic follicles (10) may be compatible with the above results if Mfge8 were secreted by FDCs and trapped by TBMφs. We tested this proposition in reciprocal BM chimeras between *Mfge8*$^{-/-}$ and WT mice. FDCs are stromal and radioresistant, whereas TBMφs are mononuclear phagocytes of hematopoietic origin and are thought to be radiosensitive (14). To provide an independent histogenetic marker, lethally irradiated *Mfge8*$^{-/-}$ mice expressing the CD45.2 allelic variant were reconstituted with BM from CD45.1 congenic WT mice, and vice versa.

The mean reconstitution efficiency determined by FACS analysis of peripheral blood was 93.8 ± 3.6% (unpublished

data). The donor origin of TBMφs was confirmed by multi-color immunofluorescence with antibodies against CD45.1, CD45.2, and CD68 in >50 follicles of five mice per group. The results ruled out the possibility that host-derived TBMφs may have survived irradiation (Fig. S2, available at http://www.jem.org/cgi/content/full/jem.20071019/DC1). Immuno-

stains of *Mfge8⁻/⁻*→*Mfge8⁻/⁻* (all CD45.2⁺) and WT→WT (all CD45.1⁺) spleens confirmed the absence of cross-reactivity (Fig. S2). Two-color immunolabeling of *Mfge8⁻/⁻*→WT spleens with antibodies against CD68 (cyan) and CD45.1 (red) confirmed that TBMφs were not host derived, whereas TBMφs of WT→*Mfge8⁻/⁻* spleens did not express CD45.2 (Fig. S2).
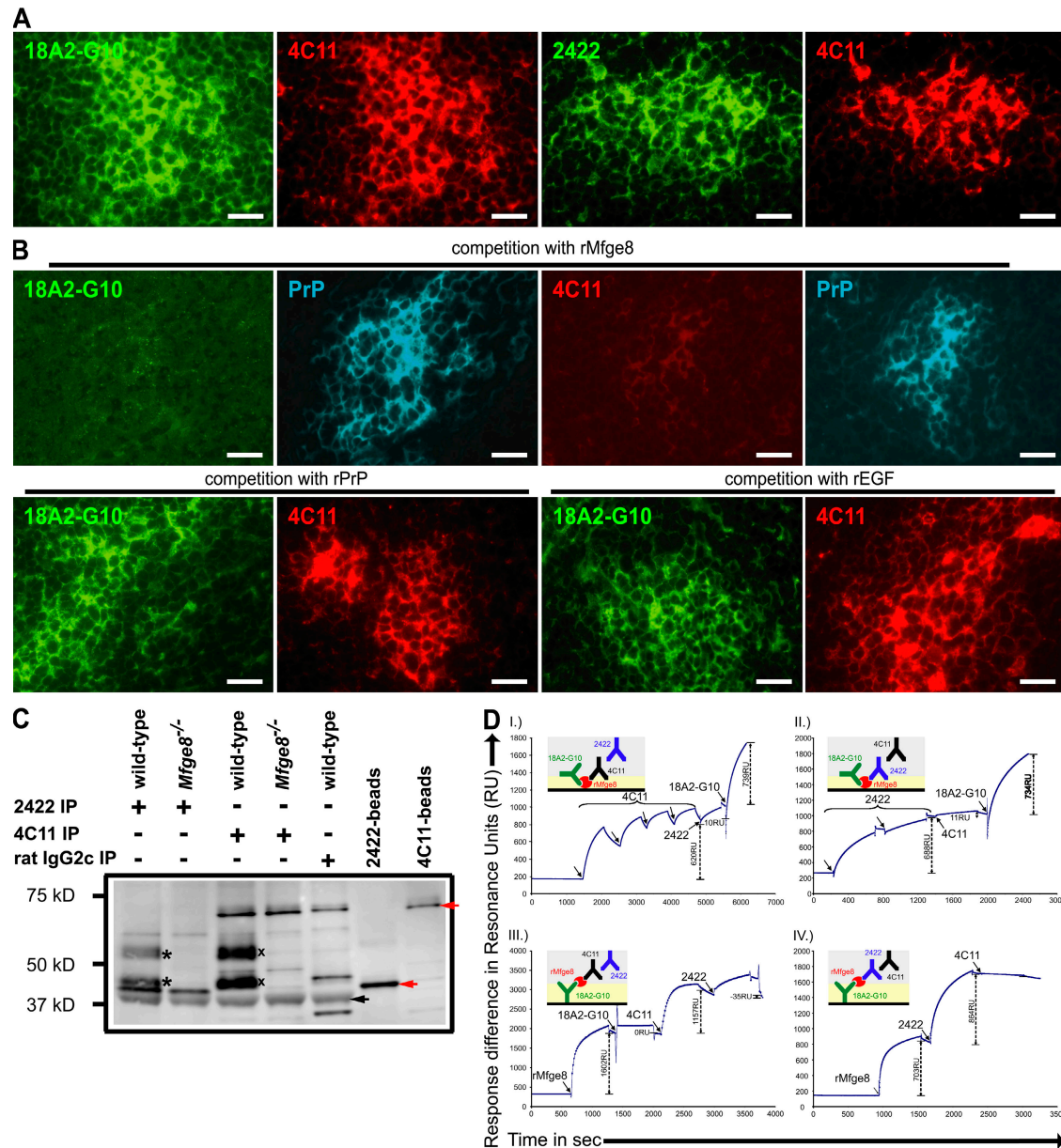

Figure 1. FDC–M1 and Mfge8 are identical. (A) Two-color immunolabeling of a WT spleen stained with anti-Mfge8 antibody 18A2-G10 (green) and anti–FDC-M1 antibody 4C11 (red), or anti-Mfge8 antibody 2422 (green) and 4C11 (red). Both anti-Mfge8 antibodies showed colocalization with 4C11. (B) Preincubation with 25 µg/ml rMfge8 blocked the labeling of FDCs with 18A2-G10 or 4C11. To visualize FDCs, sections were stained with anti-PrP antibody POM2. For control, sections were preincubated with rEGF or rPrP. Bars, 100 µm. (C) Splenic protein extracts (WT and *Mfge8⁻/⁻*) were immunoprecipitated with 2422 or 4C11, or to a rat IgG2c isotype control antibody. Control beads were coupled with 2422 or 4C11 but were not exposed to splenic extracts. Western blots were probed with 18A2-G10. Mfge8-specific bands are indicated (* and x). Arrows indicate nonspecific bands. (D) Sensograms indicating binding of each protein after subtraction of their binding to a control protein-coupled surface. Black arrows indicate antibody injections. (insets) Schematic representations of binding and competition events. For control, injections of all proteins were made on two flow cells, with one cell coated with control protein and another coated with the protein of interest.

JEM

Therefore, in all chimeras the overwhelming majority of TBMφs always originated from donor BM.

Early analyses of BM chimeras suggested a hematopoietic derivation of FDCs (15), but most current evidence favors a stromal origin (14, 16). Indeed, *Ptprc*, which encodes CD45, was markedly reduced in MACS–enriched FDC clusters (17), whereas *Mfge8* and *Cxcl13* (a B cell–attracting chemokine expressed by FDCs; reference 18) were increased
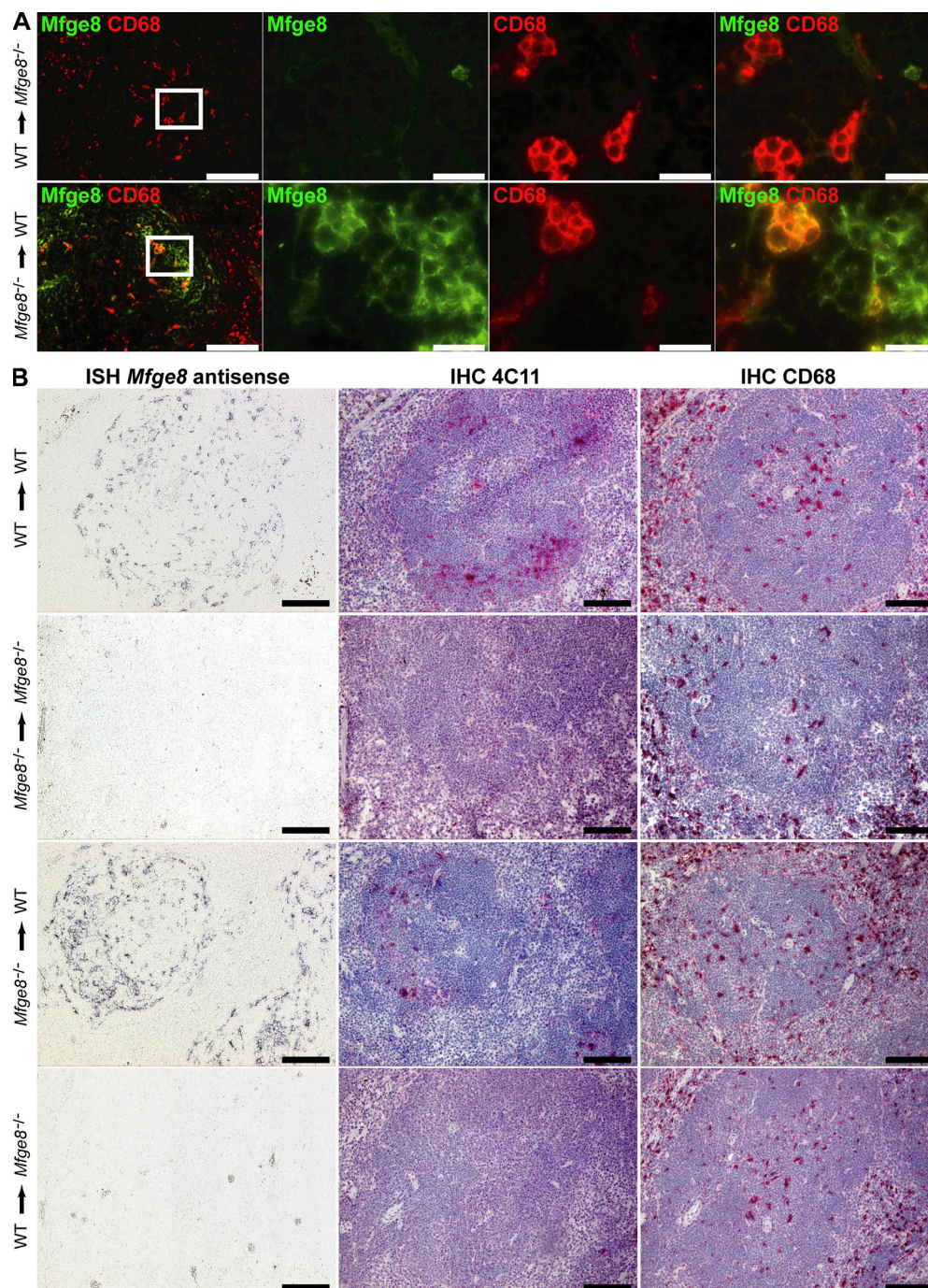

Figure 2. Analysis of splenic *Mfge8* expression by immunofluorescence and ISH. (A) BM chimeras were stained with anti-Mfge8 antibody (clone 2422; green) and anti-CD68 antibody (red). Mfge8 immunoreactivity of FDCs and CD68+ TBMφs was only observed when FDCs were of WT origin. Figures show areas inside follicles. White squares mark the areas shown at a higher magnification. Bars, 20 μm. (B) Splenic *Mfge8* expression was assessed by ISH. Consecutive sections were immunolabeled with 4C11 and anti-CD68. *Mfge8* expression and 4C11 immunostaining was only found in WT mice irrespective of the BM genotype (top and second from bottom). *Mfge8*−/− mice receiving BM from either *Mfge8*−/− or WT mice showed no *Mfge8*-specific signal after ISH and no 4C11 immunostaining. Bars, 100 μm.

1296   FDCS AND TBMφS COOPERATE IN APOPTOTIC CELL REMOVAL | Kranich et al.

(Fig. S3, available at http://www.jem.org/cgi/content/full/jem.20071019/DC1). We conclude that FDCs do not express CD45, and were therefore not identifiable as host derived in CD45.1/CD45.2 immunostains.

BM-chimeric mice were immunized and boosted with OVA/alum to induce GCs before analysis. 9 wk after reconstitution, splenic Mfge8 and CD68 expression were analyzed immunohistochemically. Surprisingly, *Mfge8⁻/⁻* mice that had received WT BM (WT→*Mfge8⁻/⁻*) completely lacked splenic Mfge8 immunoreactivity. Not only radioresistant FDCs but also BM-derived CD68⁺ TBMϕs were phenotypically Mfge8 negative (Fig. 2 A, top) although they had clearly originated from *Mfge8⁺/⁺* donors (Fig. S2). In contrast, spleens of WT mice reconstituted with *Mfge8⁻/⁻* BM (*Mfge8⁻/⁻*→WT) contained not only Mfge8⁺ FDCs but also phenotypically Mfge8-positive TBMϕs originating from *Mfge8⁻/⁻* donors (Fig. 2 A). Irrespective of their genotype, therefore, TBMϕs were always Mfge8⁺ whenever FDCs expressed Mfge8, yet they were always Mfge8⁻ whenever FDCs lacked Mfge8.

We then determined the transcriptional patterns of splenic *Mfge8* by RNA ISH. In WT→WT mice, *Mfge8* transcription was restricted to follicles (Fig. 2 B) and was strongest in GCs, where FDCs reside. Some Mfge8⁺ cells were found in the periphery of follicles. These cells were radioresistant and may represent immature FDC precursor cells (19). Overall, the ISH visualized more Mfge8⁺ cells than 4C11 immunohistochemistry, probably owing to the higher sensitivity of the former.

Consecutive sections were immunostained with 4C11 and anti–CD68 antibodies. In this case, both Mfge8 immunostains and *Mfge8* ISH visualized characteristic FDC networks, confirming that Mfge8 is indeed produced by FDCs rather than being secreted by other cell types and taken up by FDCs (Fig. 2 B). No ISH signal was detected on *Mfge8⁻/⁻*→*Mfge8⁻/⁻* chimeric spleens, confirming the specificity of the *Mfge8* in situ riboprobe (Fig. 2 B).

The *Mfge8* expression pattern in *Mfge8⁻/⁻*→WT chimeras was identical to that of WT mice, whereas *Mfge8* expression was completely absent from WT→*Mfge8⁻/⁻* chimeras (Fig. 2 B). Therefore, radioresistant cells including FDCs, rather than radiosensitive cells including TBMϕs, are the source of Mfge8 in the spleen. *Mfge8* expression in WT→*Mfge8⁻/⁻* chimeric spleens was below detectability by quantitative RT-PCR (<0.25% WT splenocyte RNA spiked into *Mfge8⁻/⁻* splenocyte RNA; not depicted), whereas *Mfge8⁻/⁻*→WT spleens showed expression levels similar to WT→WT spleens (Fig. S4 A, available at http://www.jem.org/cgi/content/full/jem.20071019/DC1).

We then searched for *Mfge8* transcripts within CD68⁺ macrophages by combining fluorescent ISH (green) with CD68 immunofluorescence stains on individual cryosections (Fig. S4 B). In immunized WT spleens, none of the CD68⁺ TBMϕs (white arrows) colocalized with the green *Mfge8* ISH signal, which was absent in the *Mfge8⁻/⁻* spleens. Conversely, all cells showing *Mfge8* transcripts were negative in the CD68 immunostaining (Fig. S4 B, yellow arrows). Hence, FDCs but not TBMϕs transcribe *Mfge8*.

PMϕs express Mfge8 only upon stimulation

PMϕs were previously found to express *Mfge8* upon stimulation with thioglycollate (11). We analyzed *Mfge8* expression in stimulated PMϕs isolated from BM chimeras. *Mfge8* expression was only detectable in PMϕs from WT→WT and WT→*Mfge8⁻/⁻* chimeras but not in those of *Mfge8⁻/⁻*→WT and *Mfge8⁻/⁻*→*Mfge8⁻/⁻* chimeras, and was only detectable in stimulated but not in unstimulated cells (Fig. S5, available at http://www.jem.org/cgi/content/full/jem.20071019/DC1). These results confirm that extralymphatic PMϕs do not express *Mfge8* under normal conditions but only after stimulation (11).

Naive, nonimmunized mice displayed *Mfge8*-expressing FDC networks, implying that FDCs express *Mfge8* constitutively. In contrast, *Mfge8* transcription by PMϕ appears to be dependent on inflammatory stimuli and was never detectable in vivo in TBMϕs, not even after immunization, when most TBMϕs are highly immunoreactive for secondarily acquired Mfge8 protein.

TBMϕs can acquire Mfge8 from extracellular sources

The above indicates that TBMϕs appear immunohistochemically Mfge8⁺ because they take up FDC-derived Mfge8, either before or during the ingestion of apoptotic B cells. To further challenge this hypothesis, 10 μg rMfge8 or rPrP was injected into the footpads of *Mfge8⁻/⁻* or *Prnpº/º* mice, respectively. 20 h later, the draining popliteal lymph nodes were collected and immunostained for Mfge8. Although no Mfge8 immunolabeling was observed in the contralateral lymph node after PBS injection (Fig. 3, middle), Mfge8 was readily detectable in draining lymph nodes after Mfge8 injection. FDC networks, visualized by immunofluorescence for the complement receptors CD21/35, were only weakly Mfge8⁺ (Fig. 3, left), indicating that they trapped only small amounts of Mfge8. In contrast, CD68⁺ TBMϕs were strongly immunoreactive for Mfge8. No PrP immunoreactivity was observed in the draining lymph nodes of *Prnpº/º* mice 20h after injection (Fig. 3, right), indicating that TBMϕs do not generically incorporate all soluble recombinant proteins. We conclude that Mfge8 is synthesized by FDCs, secreted, and eventually acquired by macrophages exposing appropriate receptors.

Lack of Mfge8 expression by FDCs impairs corpse engulfment

Mfge8⁻/⁻ mice suffer from splenomegaly and a phagocytosis defect of TBMϕs (10). We used BM chimeras to determine whether these phenotypes are caused by stromal or hematopoietic *Mfge8* deficiency. Only *Mfge8⁻/⁻*→*Mfge8⁻/⁻* and WT→*Mfge8⁻/⁻* mice developed splenomegaly, with spleen weights approximately twice as high as those of WT→WT and *Mfge8⁻/⁻*→WT mice (Fig. S6, available at http://www.jem.org/cgi/content/full/jem.20071019/DC1). Therefore, the splenomegaly of aged *Mfge8⁻/⁻* mice could be unambiguously ascribed to the lack of *Mfge8* expression by stromal cells,

and could not be corrected by any putative hematopoietic *Mfge8* expression.

Mfge8$^{-/-}$ spleens were found to host enlarged TBMφs, whose surfaces were loaded with nonengulfed apoptotic bodies (10). In light of the above results, this phenotype may be attributed to the absence of FDC-produced Mfge8. We tested this possibility by quantifying the number of TdT-mediated dUTP-biotin nick-end labeling (TUNEL)–positive apoptotic cells associated with each TBMφ. We first determined the mean number of TUNEL$^+$ cells associated with all macrophages within splenic white pulp follicles. *Mfge8*$^{-/-}$→*Mfge8*$^{-/-}$ and WT→*Mfge8*$^{-/-}$ chimeras displayed marginally increased numbers of macrophage-bound apoptotic cells over WT→WT and *Mfge8*$^{-/-}$→WT chimeras (unpublished data), but statistical significance was not attained. We then performed the same analysis but counted only those macrophages that resided within PNA$^+$ GCs. The mean number of TUNEL$^+$ apoptotic

cells per CD68$^+$ TBMφ was determined in at least 13 PNA$^+$ GCs in each group of mice. TBMφs of *Mfge8*$^{-/-}$→*Mfge8*$^{-/-}$ and WT→WT mice were found to be associated with 6 ± 1.8 and 2.4 ± 0.5 TUNEL$^+$ cells, respectively. TBMφs of WT→*Mfge8*$^{-/-}$ mice were associated with significantly more TUNEL$^+$ cells (5.8 ± 1.6) than TBMφs of *Mfge8*$^{-/-}$→WT mice (2.5 ± 0.9; P < 0.0001; Fig. 4 A). We conclude that the apoptotic load of macrophages was increased whenever Mfge8 was absent from radioresistant stromal cells, supporting the contention that FDC-derived Mfge8 regulates the engulfment of apoptotic cells.

We found apoptotic lymphocytes in various degradation stages within TBMφs of all chimeric mice, including *Mfge8*$^{-/-}$→*Mfge8*$^{-/-}$ mice (Fig. 4 B). This points to the existence of hitherto unexplored, Mfge8-independent mechanisms of corpse removal and may explain why *Mfge8*$^{-/-}$ mice only suffer from mild SLE. Complement factors may also be
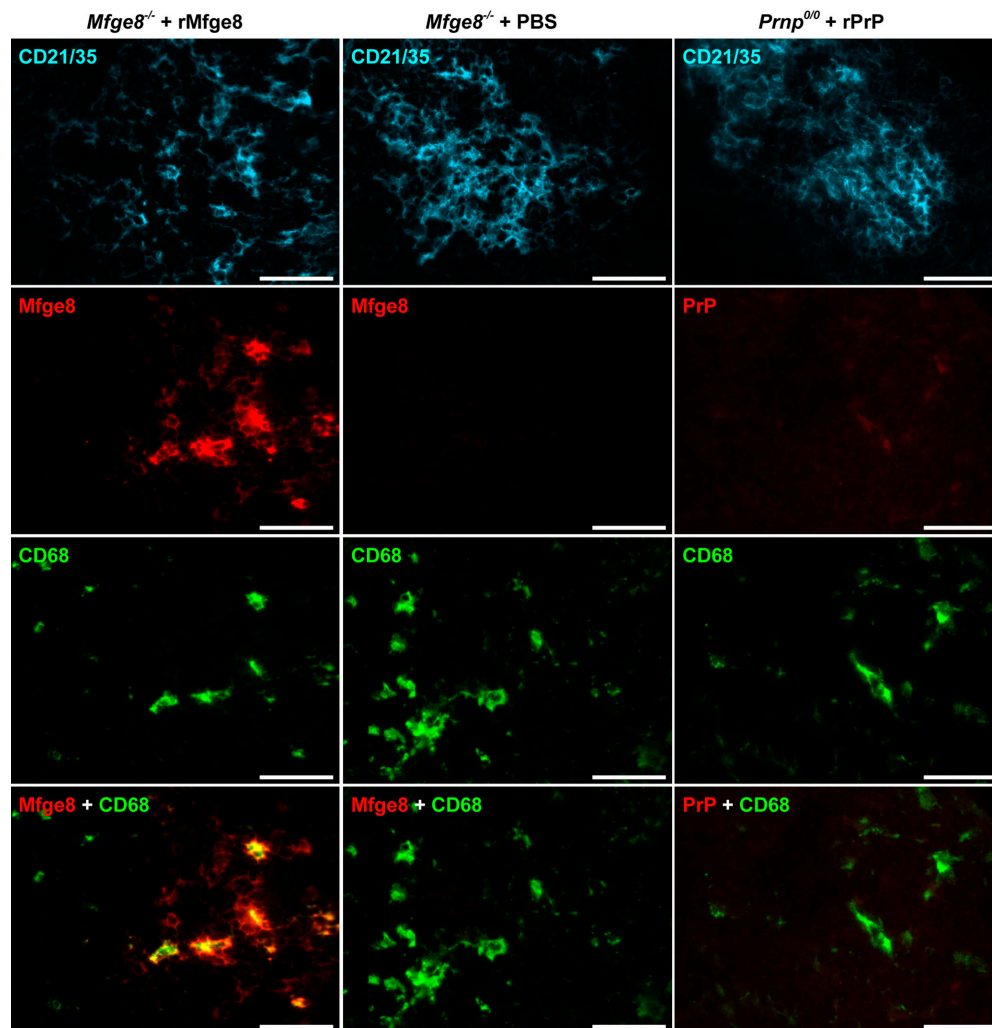

Figure 3. TBMφs bind extracellular Mfge8. Footpads of *Mfge8*$^{-/-}$ mice were injected with 10 μg rMfge8. For control, PBS or rPrP was injected into the contralateral footpad of *Prnp*$^{o/o}$ mice. 20 h later, popliteal lymph nodes were collected and analyzed by immunofluorescence with anti-Mfge8 and anti-PrP antibodies. TBMφs and FDCs showed strong and weak Mfge8 staining, respectively. rPrP was undetectable in the lymph nodes of *Prnp*$^{o/o}$ mice. Bars, 50 μm.

involved, because FDCs are a source of splenic C1q (20) and *C1q*-ablated mice develop SLE (21).

Efficient degradation of apoptotic cells in splenic follicles depends on LT signaling

Because FDC development and maintenance require LT signaling, LTs may control *Mfge8* availability and, consequently, removal of apoptotic cells from GCs. We tested this prediction in $Ltbr^{-/-}$, $Lta^{-/-}$, and $Ltb^{-/-}$ mice, whose splenic follicles contain PNA⁺ clusters and few IgM^low^IgD⁺ B cells (22) but are disorganized and contain no FDCs (23). We found splenic *Mfge8* to be decreased almost 200-fold in $Ltbr^{-/-}$ mice and ~70–90-fold in $Lta^{-/-}$ and $Ltb^{-/-}$ mice (Fig. S7, available at http://www.jem.org/cgi/content/full/jem.20071019/DC1). We then compared the prevalence of TBMϕ-associated apoptotic cells in the spleens of $Ltbr^{-/-}$,
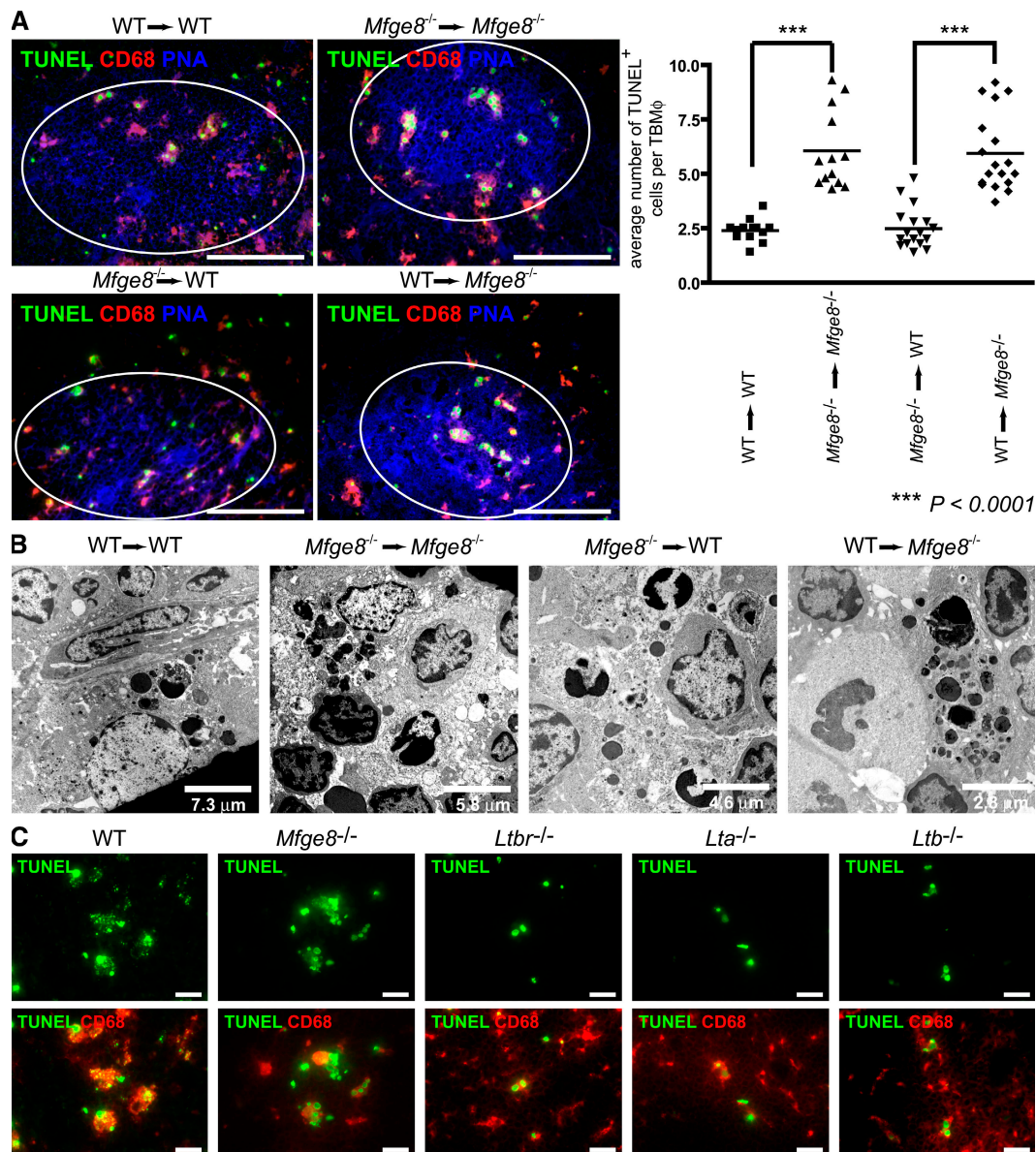

Figure 4.   **Impaired engulfment of apoptotic bodies in the absence of stromal Mfge8.** (A) Apoptotic cells, TBMϕs, and GCs were visualized by TUNEL, anti-CD68, and PNA, respectively, on splenic cryosections 9 wk after BM reconstitution and after immunization. (right) Each datapoint represents the mean number of TUNEL⁺ cells per TBMϕ in one individual GC. $Mfge8^{-/-} \rightarrow Mfge8^{-/-}$ and WT→$Mfge8^{-/-}$ mice showed increased numbers of TUNEL⁺ cells per TBMϕ. Horizontal bars represent means. White circles (left) indicate GCs. Bars, 100 µm. (B) Ultrastructural features of TBMϕs of aged BM-chimeric mice 41 wk after reconstitution. Apoptotic cells in various degradation stages were observed inside TBMϕs of all chimeric mice. (C) Engulfment of apoptotic cells by TBMϕs in WT, $Mfge8^{-/-}$, $Ltbr^{-/-}$, $Lta^{-/-}$, and $Ltb^{-/-}$ mice was analyzed by TUNEL (green) and CD68 (red) staining. WT TBMϕs contained copious TUNEL⁺ material. The latter was also observed in $Mfge8^{-/-}$ mice, but most TUNEL⁺ cells were large and intact. $Ltbr^{-/-}$, $Lta^{-/-}$, and $Ltb^{-/-}$ macrophages were small and only contained intact TUNEL⁺ cells. At least three mice per genotype and ≥10 follicles per mouse were analyzed. Bars, 20 µm.
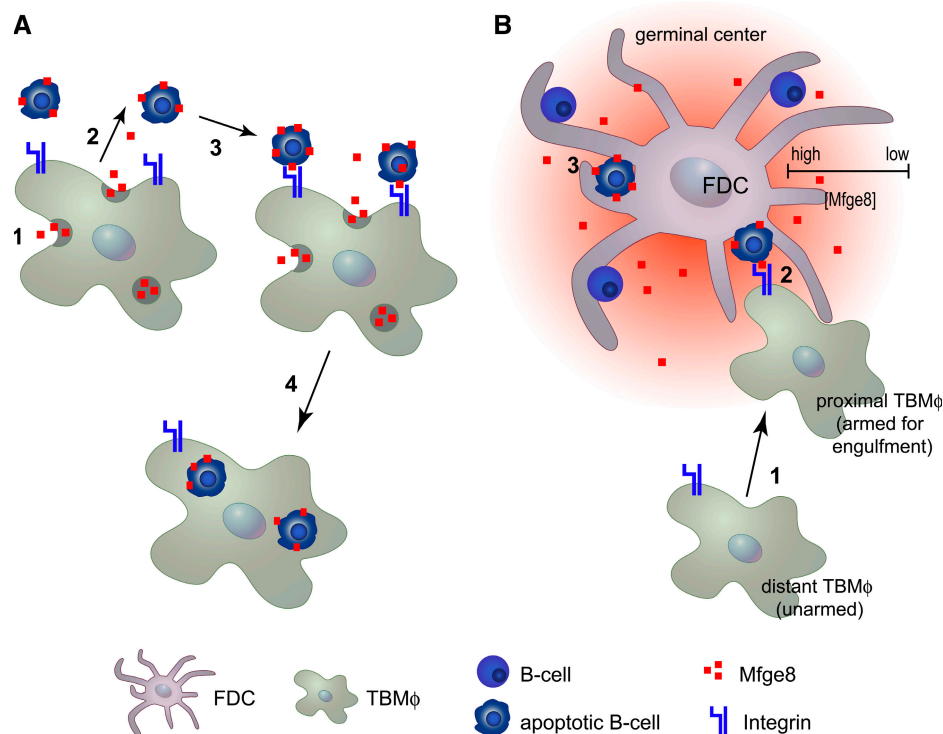
Figure 5. Mfge8–dependent removal of apoptotic cells from the GC. (A) In acute inflammatory conditions, macrophages secrete *Mfge8* (step 1; reference 30), which targets apoptotic bodies (step 2) and allows macrophages to bind them via integrins (step 3). The Mfge8–integrin interaction results in engulfment (step 4). (B) Revised model of splenic Mfge8-dependent engulfment. In this case, Mfge8 is not produced by macrophages but by FDCs. These establish a local Mfge8 gradient within GCs (step 1). TBMϕs are therefore licensed for selective engulfment at the sites of apoptosis (step 2). Apoptotic cells are presumably decorated by Mfge8 while in contact with FDCs (step 3).

Lta$^{-/-}$, and *Ltb*$^{-/-}$ mice immunized with OVA (Fig. 4 C). TBMϕs of WT mice contained tingible bodies identifiable as small TUNEL$^+$ particles inside TBMϕs (Fig. 4 C, far left). Small degraded TUNEL$^+$ bodies were also observed in *Mfge8*$^{-/-}$ mice (Fig. 4 C, second from the left). In contrast, although *Ltbr*$^{-/-}$ follicles contained some CD68$^+$ cells binding TUNEL$^+$ cells, the latter appeared largely intact, and the accumulation of small characteristic TUNEL$^+$ tingible bodies within TBMϕs was absent (Fig. 4 C). Similar results were observed in mice devoid of LTα or LTβ (Fig. 4 C), confirming a severe impairment of macrophage-mediated degradation of apoptotic cells in the GCs of all mice defective in LT signaling.

The realization that FDCs are the major source of Mfge8 in GCs points to a previously unrecognized role for these cells in GC homeostasis. In addition to modulating the survival of GC B cells, FDCs appear to regulate their removal once these cells have undergone apoptosis. These results indicate that FDCs provide Mfge8 to GCs, which then binds to phosphatidylserine on apoptotic B cells and targets them for removal by TBMϕs. This would explain why TBMϕs register as Mfge8$^+$ upon ingestion of apoptotic B cells, and indeed, we were able to show that TBMϕs take up extracellular Mfge8 after subcutaneous injection of rMfge8 (Fig. 3).

This model predicates a functional interaction of two distinct cell types, FDCs and TBMϕs, in the removal of apoptotic cells from GCs. This is plausible for physiological and anatomical reasons. Apoptosis of GC B cells is very frequent, and their rapid and efficient removal seems important to avoid autoimmunity. But the paucity of scavenging cells, TBMϕs, may limit the removal process. However, it would be wasteful for TBMϕs to produce both Mfge8 and its receptors, $\alpha_V\beta_3$ and $\alpha_V\beta_5$ integrins. Conversely, these data suggest a tunable mechanism, with FDCs establishing a gradient of Mfge8 availability within GCs. Through their strategic microanatomical positioning within follicles, FDCs arm TBMϕs for engulfment only in the vicinity of apoptotic B cells. Accordingly, the apoptotic body load was dramatically increased in macrophages residing within GCs. Because of their intimacy with GC B cells, FDCs may directly decorate negatively selected B cells with Mfge8 (Fig. 5). This two-tiered mechanism may help ensure that numerous dying cells are recognized and degraded by far fewer TBMϕs.

Lack of LT signaling, which results in the absence of FDCs, suppressed splenic *Mfge8* expression, and combined TUNEL assays and CD68 immunostains indicated that the efficient removal of apoptotic cells was also impaired. These findings hint to a signaling hierarchy that is driven by LTs, enrolls LTβR-dependent signaling within FDCs, and enables topographically controlled apoptotic cell removal within GCs.

Ltbr$^{-/-}$, *Lta*$^{-/-}$, and *Ltb*$^{-/-}$ mice develop severe systemic autoimmunity with lymphocytic infiltrates in multiple organs. Although this disease is more severe than that of *Mfge8*$^{-/-}$ mice, the similarities are evident and include elevated levels of autoimmune antibodies and renal pathology (10, 24). In LT–deficient mice, this phenotype was originally attributed to decreased *Aire* expression in medullary thymic epithelial cells (24). This view, however, was challenged by reports of unaltered frequencies of *Aire*$^+$ medullary thymic epithelial cells in *Lta*$^{-/-}$ mice (25) and unaltered *Aire* expression in *Ltbr*$^{-/-}$ mice (26, 27). Our findings suggest an alternative explanation for the autoimmunity in the latter mice. By depleting follicular Mfge8, LT signaling defects suppress the licensing activity that FDCs exert on TBMϕs and, in turn, impair corpse removal from GCs. Hence, FDCs may control housekeeping functions required for the operation of lymphoid organs and for avoiding autoimmune phenomena.

MATERIALS AND METHODS

Mice. *Mfge8*$^{-/-}$ mice were generated in the laboratory of S. Nagata (Kyoto University, Kyoto, Japan) and were bred on a (C57BL/6 × 129)F$_1$ mixed background (10). *Prnp*$^{o/o}$ mice and *Ltbr*$^{-/-}$, *Lta*$^{-/-}$, and *Ltb*$^{-/-}$ mice were described previously (22, 28, 29). C57BL/6-CD45.1 mice were obtained from Harlan Laboratories. All experiments were in accordance with Swiss federal legislation and were approved by local authorities.

Immunohistochemical analysis. Acetone-fixed cryosections were blocked (0.5% BSA, 1% goat serum in PBS) and primary antibodies were added. Primary antibodies were 4C11 (NovImmune SA or BD Biosciences), 18A2-G10 (MBL International), 2422 (Qbiogene), anti-CD21/35, anti-CD45.2–FITC, anti-CD45.1–biotin (all from BD Biosciences), anti-CD68 (AbD Serotec), and anti-PrP antibody POM2-Cy5 (developed in our laboratory). For competition experiments, 18A2-G10 or 4C11 were preincubated with 25 μg/ml rMfge8, rEGF (both from R&D Systems), or rPrP (produced in our laboratory). Sections were analyzed by fluorescence microscopy (BX61; Olympus). TUNEL assays were performed with the ApopTaq Plus Fluorescein In Situ Apoptosis Detection Kit (Millipore) according to the manufacturer's instructions. Before TUNEL stainings, unfixed sections were blocked and stained with biotinylated PNA (Vector Laboratories) and anti-CD68 antibodies, and then fixed with paraformaldehyde. Quantitation of TUNEL$^+$ cells per macrophage was performed in a stringently blinded fashion. One scientist recorded micrographs of GCs, and a second scientist (blinded with respect to the genotypes of the mice) counted the number of apoptotic bodies per macrophage.

Immunoprecipitation and Western blotting. Paramagnetic beads (Dynabeads M280 Tosylactivated; Invitrogen) were conjugated with 4C11, 2422, or rat IgG2c isotype control antibody according to the manufacturer's manual and incubated with spleen homogenates. Immunoprecipitates were analyzed by Western blotting using anti–Mfge8 antibody 18A2-G10. For detection, goat anti–Armenian hamster IgG–horseradish peroxidase was used.

SPR. SPR was performed on a Biacore 3000 instrument (GE Healthcare). Antibodies or recombinant proteins were immobilized on flow cells of an activated CM5 chip (Biacore) to 10,000 and 15,000 response units, respectively. All recombinant proteins or antibodies were injected at a concentration of 50 μg/ml diluted in HBS-EP buffer. The flow rate was 5 μl/min. For control, all protein injections were made on two flow cells, where the first flow cell was coated with control protein/antibody and the second was coated with the protein/antibody of interest.

BM chimeras. BM recipients were lethally irradiated (950 rad). Donor BM was isolated by flushing tibias and femurs. Recipient mice received 10^7 donor BM cells i.v. Reconstitution efficiency was assed after 5 wk by FACS analysis of blood leukocytes. 6 wk after engraftment, mice were immunized i.p. with 100 μg OVA (Sigma-Aldrich) in alum (Imject Alum; Thermo Fisher Scientific). 2 wk later, mice were boosted with the same dose of OVA.

RNA ISH. Digoxigenin (DIG)-labeled *Mfge8* riboprobe was obtained by transcription of pBluescript II KS+ (Stratagene) containing the open reading frame of *Mfge8*. ISH was performed on spleen cryosections. For fluorescent ISH, sections were prestained with biotinylated anti-CD68 antibody and postfixed in 4% paraformaldehyde, followed by acetylation. After prehybridization, 200 ng/ml of DIG-labeled RNA probe was added to the hybridization buffer and incubated at 72°C overnight. For detection, either anti-DIG–alkaline phosphatase or anti-DIG–fluorescein antibody with a fluorescent enhancer kit (Roche) was used.

FDC cluster isolation and quantitative real-time PCR analysis. FDCs from lymph nodes were isolated as described previously (17). FDC-enriched and flow-through fractions were lysed in TRIzol. RNA was isolated and cDNA was synthesized. Quantitative real-time PCR was performed using the SYBR Green PCR Master Mix (QIAGEN) on a 7900HT Fast Real-Time PCR System (Applied Biosystems) using the default cycling conditions. Expression levels were normalized using *Gapdh*. The following primers were used: *Gapdh* forward primer, 5′-CCACCCCAG-CAAGGAGACT-3′; *Gapdh* reverse primer, 5′-GAAATTGTGAGGGA-GATGCT-3′; *Mfge8* forward primer, 5′-ATATGGGTTTCATGGGC-TTG-3′; *Mfge8* reverse primer, 5′-GAGGCTGTAAGCCACCTTGA-3′; *Cxcl13* forward primer, 5′-TCGTGCCAAATGGTTACAAA-3′; *Cxcl13* reverse primer, 5′-ACAAGGATGTGGGTTGGGTA-3′; *Ptprc* forward primer, 5′-AAACGATCGGTGACTTTTGG-3′; and *Ptprc* reverse primer, 5′-AGCTCTTCCCCTTTCCATGT-3′.

Electron microscopy. Samples were fixed in 2% glutaraldehyde in 0.1 M cacodylate buffer (pH 7.4), washed and postfixed in a mixture of 1% OsO$_4$ and 1.5% K$_4$Fe(CN)$_6$ in 0.1 M cacodylate buffer (pH 7.4), dehydrated, and embedded in Epon 812 (Fluka). The resin specimens were trimmed, and 70–90-nm sections were cut. Ultrathin sections were collected on copper 6200 grids and contrasted with uranyl acetate and lead acetate before examination with a transmission electron microscope (CX 100 II; JEOL Ltd.).

Online supplemental material. Fig. S1 shows that *Mfge8*$^{-/-}$ mice lack FDC-M1$^+$ networks. Fig. S2 reveals that TBMϕs are donor derived. Fig. S3 depicts *Ptprc* expression as down–regulated in FDC-enriched clusters. Fig. S4 shows that *Mfge8* expression is absent in spleens with stromal *Mfge8* deficiency and that CD68$^+$ TBMϕs do not contain *Mfge8* RNA. An analysis of *Mfge8* expression in PMϕs is depicted in Fig. S5. Fig. S6 shows that stromal *Mfge8* deficiency causes splenomegaly. Fig. S7 demonstrates that splenic *Mfge8* expression depends on LT signaling. Online supplemental material is available at http://www.jem.org/cgi/content/full/jem.20071019/DC1.

REFERENCES

1. Chen, L.L., J.C. Adams, and R.M. Steinman. 1978. Anatomy of germinal centers in mouse spleen, with special reference to "follicular dendritic cells". *J. Cell Biol.* 77:148–164.
2. Tew, J.G., G.J. Thorbecke, and R.M. Steinman. 1982. Dendritic cells in the immune response: characteristics and recommended nomenclature

(A report from the Reticuloendothelial Society Committee on Nomenclature). *J. Reticuloendothel. Soc.* 31:371–380.

3. Tew, J.G., J. Wu, M. Fakher, A.K. Szakal, and D. Qin. 2001. Follicular dendritic cells: beyond the necessity of T-cell help. *Trends Immunol.* 22:361–367.

4. Klaus, G.G., J.H. Humphrey, A. Kunkl, and D.W. Dongworth. 1980. The follicular dendritic cell: its role in antigen presentation in the generation of immunological memory. *Immunol. Rev.* 53:3–28.

5. Kosco-Vilbois, M.H. 2003. Are follicular dendritic cells really good for nothing? *Nat. Rev. Immunol.* 3:764–769.

6. Hannum, L.G., A.M. Haberman, S.M. Anderson, and M.J. Shlomchik. 2000. Germinal center initiation, variable gene region hypermutation, and mutant B cell selection without detectable immune complexes on follicular dendritic cells. *J. Exp. Med.* 192:931–942.

7. Matsumoto, M., S.F. Lo, C.J. Carruthers, J. Min, S. Mariathasan, G. Huang, D.R. Plas, S.M. Martin, R.S. Geha, M.H. Nahm, and D.D. Chaplin. 1996. Affinity maturation without germinal centres in lymphotoxin-alpha-deficient mice. *Nature.* 382:462–466.

8. Taylor, P.R., M.C. Pickering, M.H. Kosco-Vilbois, M.J. Walport, M. Botto, S. Gordon, and L. Martinez-Pomares. 2002. The follicular dendritic cell restricted epitope, FDC-M2, is complement C4; localization of immune complexes in mouse tissues. *Eur. J. Immunol.* 32:1888–1896.

9. Kosco, M.H., E. Pflugfelder, and D. Gray. 1992. Follicular dendritic cell-dependent adhesion and proliferation of B cells in vitro. *J. Immunol.* 148:2331–2339.

10. Hanayama, R., M. Tanaka, K. Miyasaka, K. Aozasa, M. Koike, Y. Uchiyama, and S. Nagata. 2004. Autoimmune disease and impaired uptake of apoptotic cells in MFG-E8-deficient mice. *Science.* 304:1147–1150.

11. Hanayama, R., M. Tanaka, K. Miwa, A. Shinohara, A. Iwamatsu, and S. Nagata. 2002. Identification of a factor that links apoptotic cells to phagocytes. *Nature.* 417:182–187.

12. Stubbs, J.D., C. Lekutis, K.L. Singer, A. Bui, D. Yuzuki, U. Srinivasan, and G. Parry. 1990. cDNA cloning of a mouse mammary epithelial cell surface protein reveals the existence of epidermal growth factor-like domains linked to factor VIII-like sequences. *Proc. Natl. Acad. Sci. USA.* 87:8417–8421.

13. Thielen, C., N. Antoine, F. Melot, J.Y. Cesbron, E. Heinen, and R. Tsunoda. 2001. Human FDC express PrPc in vivo and in vitro. *Dev. Immunol.* 8:259–266.

14. Humphrey, J.H., D. Grennan, and V. Sundaram. 1984. The origin of follicular dendritic cells in the mouse and the mechanism of trapping of immune complexes on them. *Eur. J. Immunol.* 14:859–864.

15. Kapasi, Z.F., D. Qin, W.G. Kerr, M.H. Kosco-Vilbois, L.D. Shultz, J.G. Tew, and A.K. Szakal. 1998. Follicular dendritic cell (FDC) precursors in primary lymphoid tissues. *J. Immunol.* 160:1078–1084.

16. Yoshida, K., M. Kaji, T. Takahashi, T.K. van den Berg, and C.D. Dijkstra. 1995. Host origin of follicular dendritic cells induced in the spleen of SCID mice after transfer of allogeneic lymphocytes. *Immunology.* 84:117–126.

17. Sukumar, S., A.K. Szakal, and J.G. Tew. 2006. Isolation of functionally active murine follicular dendritic cells. *J. Immunol. Methods.* 313:81–95.

18. Shi, K., K. Hayashida, M. Kaneko, J. Hashimoto, T. Tomita, P.E. Lipsky, H. Yoshikawa, and T. Ochi. 2001. Lymphoid chemokine B cell-attracting chemokine-1 (CXCL13) is expressed in germinal center of ectopic lymphoid follicles within the synovium of chronic arthritis patients. *J. Immunol.* 166:650–655.

19. Pasparakis, M., S. Kousteni, J. Peschon, and G. Kollias. 2000. Tumor necrosis factor and the p55TNF receptor are required for optimal development of the marginal sinus and for migration of follicular dendritic cell precursors into splenic follicles. *Cell. Immunol.* 201:33–41.

20. Schwaeble, W., M.K. Schafer, F. Petry, T. Fink, D. Knebel, E. Weihe, and M. Loos. 1995. Follicular dendritic cells, interdigitating cells, and cells of the monocyte-macrophage lineage are the C1q-producing sources in the spleen. Identification of specific cell types by in situ hybridization and immunohistochemical analysis. *J. Immunol.* 155:4971–4978.

21. Walport, M.J., K.A. Davies, and M. Botto. 1998. C1q and systemic lupus erythematosus. *Immunobiology.* 199:265–285.

22. Futterer, A., K. Mink, A. Luz, M.H. Kosco-Vilbois, and K. Pfeffer. 1998. The lymphotoxin beta receptor controls organogenesis and affinity maturation in peripheral lymphoid tissues. *Immunity.* 9:59–70.

23. Fu, Y.X., and D.D. Chaplin. 1999. Development and maturation of secondary lymphoid tissues. *Annu. Rev. Immunol.* 17:399–433.

24. Chin, R.K., J.C. Lo, O. Kim, S.E. Blink, P.A. Christiansen, P. Peterson, Y. Wang, C. Ware, and Y.X. Fu. 2003. Lymphotoxin pathway directs thymic Aire expression. *Nat. Immunol.* 4:1121–1127.

25. Rossi, S.W., M.Y. Kim, A. Leibbrandt, S.M. Parnell, W.E. Jenkinson, S.H. Glanville, F.M. McConnell, H.S. Scott, J.M. Penninger, E.J. Jenkinson, et al. 2007. RANK signals from CD4+3− inducer cells regulate development of Aire-expressing epithelial cells in the thymic medulla. *J. Exp. Med.* 204:1267–1272.

26. Boehm, T., S. Scheu, K. Pfeffer, and C.C. Bleul. 2003. Thymic medullary epithelial cell differentiation, thymocyte emigration, and the control of autoimmunity require lympho–epithelial cross talk via LTβR. *J. Exp. Med.* 198:757–769.

27. Venanzi, E.S., D.H. Gray, C. Benoist, and D. Mathis. 2007. Lymphotoxin pathway and Aire influences on thymic medullary epithelial cells are unconnected. *J. Immunol.* 179:5693–5700.

28. Bueler, H., M. Fischer, Y. Lang, H. Bluethmann, H.P. Lipp, S.J. DeArmond, S.B. Prusiner, M. Aguet, and C. Weissmann. 1992. Normal development and behaviour of mice lacking the neuronal cell-surface PrP protein. *Nature.* 356:577–582.

29. Koni, P.A., R. Sacca, P. Lawton, J.L. Browning, N.H. Ruddle, and R.A. Flavell. 1997. Distinct roles in lymphoid organogenesis for lymphotoxins alpha and beta revealed in lymphotoxin beta–deficient mice. *Immunity.* 6:491–500.

30. Zullig, S., and M.O. Hengartner. 2004. Cell biology. Tickling macrophages, a serious business. *Science.* 304:1123–1124.